Proceedings of ASME Turbo Expo 2014: Turbine Technical Conference and Exposition
GT2014
June 16–20, 2014, Düsseldorf, Deutschland

GT2014-25472

EXPERIMENTAL AND NUMERICAL INVESTIGATION OF A HYDROGEN COMBUSTION CHAMBER UNDER VARIOUS INLET CONDITIONS

Heidemarie Malli, Kurt Eckerstorfer, Oliver Borm
Institute for Thermal Turbomachinery and Machine Dynamics
Graz University of Technology
Inffeldgasse 25A
A-8010 Graz, Österreich
malli@tugraz.at

Peter Leitl
bionic surface technologies GmbH
Klosterwiesgasse 67
A-8010 Graz, Österreich

ABSTRACT

Flameless combustion, MILD (moderate or intense low oxygen dilution) combustion and HiTAC (high temperature air combustion) all refer to a combustion regime characterized by high temperatures and a high dilution of reactants. In most cases, this is achieved by recirculating exhaust gases. This leads to comparatively low oxygen concentrations, a largely uniform temperature field and to a drastically reduced NO_x formation. Up to now, the application of this combustion technology for gas turbine combustion chambers is still in an early development stage. Most investigations of flameless or MILD combustion chambers have been carried out for methane or certain fuel blends. Since this combustion technology has already successfully demonstrated low NO_x emissions without the need of premixing with its potential risks of flashback and autoignition, it might be a promising technology for hydrogen burning combustion chambers. The scope of this paper is to investigate a hydrogen combustion chamber for its NO_x emission characteristics and for its use in the flameless or MILD combustion regime. Thus, the influence of different inlet parameters (excess air ratio, thermal input of hydrogen, inlet velocity of the combustion air, pressure inside the combustion chamber) on the emission characteristics of the combustion chamber are examined experimentally. Additionally, for one operating point, a two–dimensional numerical simulation of the combustion chamber was carried out.

INTRODUCTION

In times, where environmental problems, like the greenhouse effect or acid rain, have become more and more an issue, novel combustion chambers for gas turbines should not only fulfil the requirements of high combustion efficiency, but also those of low pollutant emissions. In this regard, pure hydrogen is a fuel that needs to be taken into account. Unlike all hydrocarbon containing fuels, it releases no carbon dioxide during combustion. Moreover, many other toxic by–products, which are typically found in the exhaust gases of many fuels, are irrelevant when working with hydrogen. In fact, the only problematic species generated are oxides of nitrogen (NO_x). Those are formed from atmospheric nitrogen in dependence of combustion temperature, combustion pressure and residence time. Apart from nitrogen dioxide (NO_2), which is generated in smaller quantities, mainly nitric oxide (NO) is formed. Thus, the focus for reducing NO_2 emissions clearly lies on NO formation.

There are several different NO formation routes known, depending on the combustion characteristics [1, 2]. The prompt NO formation pathway via the Fenimore mechanism only applies to hydrocarbon fuels. Also, the fuel–bound NO generation is obviously of no relevance for hydrogen combustion. By contrast, the NO formation via NNH radicals mainly occurs in hydrogenated flames, because for this pathway H atoms are needed. There is also the NO generation via N_2O to be mentioned, which is especially relevant for lean conditions under high pressure. Due to

its comparatively low activation energy, it already occurs for lower combustion temperatures [3]. This fact does not apply to the thermal NO formation route via the Zeldovich mechanism. Here, extremely high temperatures are needed to provide the required activation energy, but once this prerequisite is met, this pathway becomes the predominant one [2,4]. For temperatures above 1600 °C, a residence time of some seconds is needed to activate the thermal NO formation pathway, whereas for temperatures above 2000 °C already several milliseconds are sufficient [5]. Thus, for many conventional combustion processes, the thermal NO formation route contributes the biggest proportion to the overall NO_x emissions.

This is the reason why many concepts aimed at reducing NO_x emissions focus on controlling the flame temperature in some way. One of them is flame cooling, where temperatures are reduced either by withdrawing energy through cooling rods, or by mixing the combustion products with cooler substances. Another method is staging, which can be divided into two- and multistaged combustion with cooling steps between the single combustion zones. Additionally, air- and fuel-staging can also be distinguished. A very common NO_x reducing method for heavy duty gas turbines is the lean premixed combustion. In order to avoid the occurrence of temperature peaks, fuel and air have to be perfectly premixed before entering the combustion chamber. The adiabatic combustion temperature can be controlled through high air excess. Another method is the recirculation of exhaust gases to achieve a reduction of flame temperature peaks. This can either be realized externally or internally, inside the combustion chamber.

One special group of methods to be mentioned consists of flameless combustion or flameless oxidation (FLOX®) [6, 5, 7], colorless distributed combustion (CDC) [8, 9], high temperature air combustion (HiTAC) [10] and moderate or intense low-oxygen dilution (MILD) [11, 12, 13]. Although many different denominations were established, all of them refer to very similar combustion processes which overlap to a great extent. To contribute to the confusion, over time the same denominations were used in different contexts, depending on the authors. But for all of these processes, high temperatures and high dilution of reactants, which is mostly induced by recirculating exhaust gases, is a prerequisite. This leads to comparatively low oxygen concentrations, a broader distributed reaction zone, a largely uniform temperature field, to lower luminous emissions of flame and of course, to a drastically reduced NO_x formation. Most differences occur because the definitions vary, depending on which characteristics a certain combustion method is focused on. For example, MILD combustion is defined as a regime where the inlet temperature of the reactant mixture is higher than its autoignition temperature. Additionally, the maximum allowable temperature increase is requested to be lower than the mixture's autoignition temperature in Kelvin [12]. As opposed to that, flameless combustion refers to a strong recirculation of hot combustion products, while the formation of (visible) flames should be avoided [7].

AIM OF THIS STUDY

The aim of this study is to develop and to evaluate a hydrogen combustion chamber, while focusing mainly on its emission characteristics. The reason for choosing hydrogen as fuel lies in its clean burning features when compared to conventional fuels, the only relevant pollutant being the oxides of nitrogen. Thus, the focus is on achieving low NO_x emissions. It is tried to obtain a MILD or flameless combustion regime in order to avoid a distinct thermal NO formation while operating the hydrogen combustion chamber. Premixed combustion is a problematic concept when working with hydrogen with its high reactivity, which also entails a high risk of autoignition and especially flashback [14].

The combustion chamber is developed by scaling an already published methane combustion chamber for flameless combustion [15,16,17] to fit into an already existing pressure casing. In the experimental part of this study, the impact of different inlet parameters on the NO_x formation is investigated. To this end, the excess air ratio, the thermal input of hydrogen, the inlet velocity of the combustion air and the pressure inside the combustion chamber are varied in different test runs. Additionally, the combustion chamber was investigated numerically using Ansys Fluent. The aim of this study was to find a suitable setup to model the investigated hydrogen combustion chamber.

DESIGN OF THE COMBUSTION CHAMBER

The main features of the cylindrical methane combustor, reported by Verissimo et al. [17], consist of the central air inlet, located on the top of the combustion chamber and the 16 circumferentially arranged fuel inlets. At the bottom, there is a convergent nozzle mounted, used as outlet of the exhaust gases. In a preliminary step, this combustor was scaled to a rectangular liner with a length of 330 mm. To obtain the air inlet diameter, the ratio of the air inlet diameter to the length of the combustion chamber was kept constant. This ratio was chosen, because the air diameter determines the penetration depth of the air jet. This is due to the fact that at constant air velocity, the momentum of the air jet increases quadratically with the diameter. Thus, also the penetration depth of the jet increases in the same order. Additionally, the ratio of the pitch circle diameter of the fuel inlets to the hydraulic combustion chamber diameter was kept constant. For the diameter of the fuel inlets,

the ratio of the air and fuel momentum flow was kept constant. Due to manufacturing issues, some of the calculated values were slightly adapted.

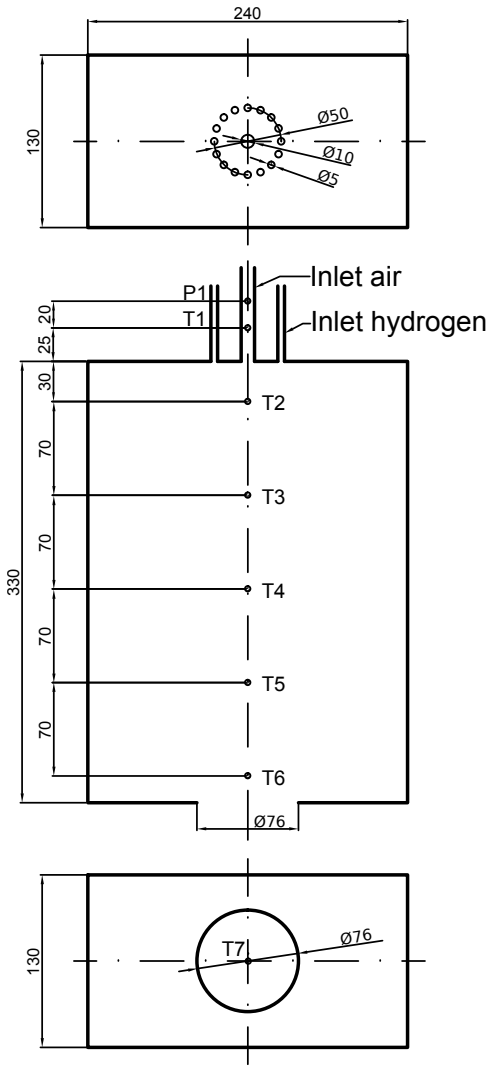

FIGURE 1. Schematic view of the instrumented hydrogen combustion chamber (please note that it was rotated clockwise by 90°)

Fig. 1 shows a schematic view of the scaled combustion chamber used for this study. The liner is rectangular with a length of 330 mm, a width of 130 mm and a height of 240 mm. On its left side, a circular air inlet with a diameter of 10 mm is located. 16 fuel inlets with a diameter of 5 mm each are arranged circumferentially around the air supply, with a pitch circle diameter of 50 mm. At the end of the liner, a plate with a central orifice of 76 mm was placed to obtain an internal exhaust gas recirculation. The fuel mass flow is controlled via a magnetic proportional valve and a mass flowmeter (Fig. 2). Additionally, the hydrogen temperature and pressure are monitored at the inlet of the annular distributor, which splits the hydrogen stream in 16 smaller fuel inlet streams.

MATERIALS AND METHODS

The main parts of the testing rig are the exhaust gas analyzer, the combustion chamber, the pressure casing, the electrical air preheater as well as the main air, the cooling air and the hydrogen supply as shown in Fig. 2. In order to conduct the experiments, the liner is integrated into the pressure casing, through which cooling air can be directed and which allows the application of higher variable pressures. In the symmetry axis of the back wall of the liner (240 x 330 mm), five temperature probes are installed from left to right, measuring the wall temperature (T2 to T6) as depicted in Fig. 1. Additionally, on the symmetry axis of the top wall of the liner (130 x 330 mm), another five temperature probes (T2' to T6') were installed. In the center of the liner exit, an additional temperature probe is mounted (T7). All used thermocouples are of type K. Inside the air inlet, the temperature and the pressure of the combustion main air are measured (T1, P1). Before entering the air preheater, the air mass flow is determined by an orifice measurement. To allow visual monitoring of the combustion process, viewing windows are integrated into the pressure casing as well as into the liner. These windows are located directly after the injectors on the front wall of the liner (240 x 330 mm) and the pressure casing, respectively. Thus, on the left side of the viewing window, the air and fuel inlets can be seen (Fig. 1).

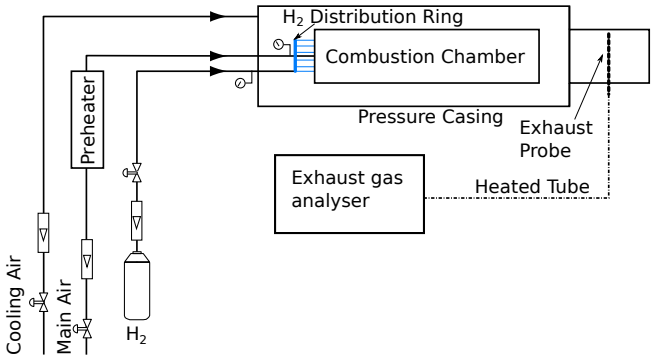

FIGURE 2. Simplified view of the experimental setup

In order to detect the exhaust gas emissions, four sampling probes are placed after the liner exit with eight bores each. The holes have a diameter of 0.3 mm and are distributed over the radius in a way that ensures that the exhaust sample gas is area weighted averaged. Due to the excess pressure inside the combustion chamber, a part of the flue gases is directed into these sampling probes and through the attached heated tubes which lead to the exhaust gas measuring unit. This unit consists of an 'ECO PHYSICS CLD 700 EL ht' NO_x analyzer based on the chemiluminescence method, and a 'MAIHAK OXOR 6N' device for the paramagnetic measurement of the O_2 concentration. The raw emission data of the NO_x analyzer is measured under hot and wet conditions and depends on the excess air coefficient as well as the amount of cooling air used for the test run. Thus, the values of the NO_x emissions are corrected to relate to a reference oxygen concentration of 15 % under dry conditions. All the calculations for the exhaust gas emissions are performed according to Borm [18].

TABLE 1. Specifications of the different test runs. For the varied parameters, the different values are separated by a semicolon. For all test runs, T_{air} is 400 K.

run	v_{air} $[\frac{m}{s}]$	λ $[-]$	P_{th} $[kW]$	p_{out} $[bar]$
0	115	2.0	30.2	2.2
1	80;115;150	1.2;1.6;2.0	30.2	-
2	115	2.0;1.6;1.2	24.15;30.2;40.2	1.8
3	115	1.2;1.6;2.0	30.2	1.3;1.8;2.2
4	115	1.6	24.15;30.2;40.2	1.4;1.8;2.3
5	80;115	1.2	30.2	-
6	115;150	2.0	30.2	-

Experimental Setup

In this set of experiments, the impact of different inlet parameters on the NO_x emissions is investigated. In several runs either the excess air ratio (λ), the thermal input of hydrogen (P_{th}), the inlet velocity of the combustion air (v_{air}) or the pressure of the combustion chamber (p_{out}) is varied. After each variation, the exhaust gas measurements are conducted after all parameters have reached a stable value as defined in Tab. 1. For each operating point, the measured values are recorded for 90 seconds. For data analysis, all values are averaged over this time span. In the first run, λ and v_{air} are varied, while keeping P_{th} and p_{out} constant. For the second run, λ and P_{th} are varied for constant v_{air} and p_{out}, which result from a constant main air mass flow. In the third run, a variation for λ and the combustion chamber outlet pressure p_{out} is performed. Thus, the main air velocity v_{air} as well as the thermal power P_{th} can be kept constant. The fourth run is carried out for varying P_{th} and p_{out}, while v_{air} and λ are constant. This resulted in a different air mass flow as well as a different fuel mass flow. For all runs, the temperature of the combustion air (T_{air}) is kept at 400 K. The mass flow of the cooling air is also held constant in a wide range. But because all obtained NO_x values are corrected as described above, a variation of the cooling air mass flow has no effect on the presented emission concentrations.

Numerical model

The combustion chamber was also investigated numerically using Ansys Fluent v.12.1, whilst the post–processing was done with ParaView v.3.14. A steady 2D axisymmetric simulation with conjugated heat transfer through the liner walls of the hydrogen combustion chamber is conducted at one operating point, listed as run 0 in Tab. 1. The unstructured mesh consists of roughly 170 k quad cells for the fluid domain and 20 k cells for the solid liner wall. The last part of the fuel and of the air inlet tubes, the combustion chamber, the cooling channel and the part of the exhaust tube leading to the emission measurement probes were simulated within the fluid domain. Because of the simplified 2D axisymmetric CFD model, the hydrogen inlet is designed annularly with the same cross–sectional area as the actual 16 fuel inlets (compare Fig. 1). For the combustion chamber, the hydraulic diameter of the actual liner is used, in order to have an optimal fit for the internal flow field. However, the cylindrical liner surface of the numerical setup is therefore roughly 30 % smaller than the rectangular one of the experimental test case. This will result in a reduced overall heat loss throughout the liner. Since the fuel and air mass flow, the overall fuel and air inlet area and the thermodynamic properties are identical for the 2D case and the actual liner, the overall momentum ratio between all fuel jets and the air jet should also remain constant in a first approximation, given that the overall boundary layer size is of the same order for the annulus and the 16 discrete hydrogen jets. Of course, with a two–dimensional axisymmetric numerical simulation, all three–dimensional effects are neglected. The largest difference in the local flow field will occur very close to the fuel injection because the 16 discrete injections will behave slightly different than the annulus injection. But still, the majority of the flow phenomena can be captured with a 2D simulation, in order to get an impression of the average flow field inside the liner. The aim of the 2D simulation was to study the behavior of different CFD chemistry

models, and this can be done numerically more efficiently using 2D simulations. Additionally, a first impression of the overall flow field inside the liner should be obtained.

In order to find a simulation model suited for the evaluation of the hydrogen combustion chamber, different combustion and turbulence models were compared. For the combustion modeling, the Eddy Dissipation Model (EDM), the Eddy Dissipation Concept Model (EDC) and the Laminar Flamelet Model were investigated. For the turbulence modeling, the Reynolds Stress Model (RSM) was applied. These different simulation models were compared for a hydrogen–air non–premixed 2D axisymmetric test case as described by Fukumoto and Ogami [19]. For the evaluation of the obtained numerical results, the published experimental data were used. On this basis, the Laminar Flamelet Model combined with the RSM Model are chosen for further numerical computations of the combustion chamber. For the Flamelet Model, 32 grid points and 10 flamelets are defined, the initial scalar dissipation rate is set to $0.01\,[1/s]$ and the step of the scalar dissipation rate is set to $5\,[1/s]$. The data used for the chemical mechanism is obtained from Shepherd [20] and is originally based on a publication from Allen [21]. As a radiation model, the P1–Model is used with a wsggm domain–based approach for the absorption coefficient. The internal and external emissivities for the wall surfaces are set to 0.7. The mass fractions of the combustion air are assumed to be 75.56% N_2, 23.15% O_2 and 1.29% Ar. To be able to compare the CFD results with the actual flames formed during the experiments, a CCD video camera is placed in front of the viewing windows. The combustion process is recorded at a frame rate of 20 fps.

EXPERIMENTAL RESULTS

The combustion chamber was operated under various inlet conditions (as specified in Tab. 1) to evaluate their impact on the formation of NO_x emissions. To this end, it is assumed that there is no unburned hydrogen present. Thus, the combustion efficiency is per definition 100% and the emission index of hydrogen (EI_{H_2}) is zero. Hence, the only remaining gaseous emissions of interest are the oxides of nitrogen. Borm [18] has conducted a sensitivity study showing that the assumption of complete combustion has no significant impact on the results of the NO_x analysis. The only thing that needs to be considered is that in order to eliminate errors due to different air flows, all measured NO_x values need to be corrected. Thus, all measured values were related to a dry oxygen content of 15%. The following four figures show the dry NO_x emissions in [ppm] for an oxygen content of 15% for different inlet parameters.

Fig. 3 shows test runs 1 to 3. For all of them the excess air coefficient was varied from a starting value of 1.2 to a final value of 2.0. For run 1, the thermal input, for run 2 the inlet velocity of the combustion air, and for run 3, both parameters were kept constant. Fig. 3 shows that the NO_x emissions increase with rising excess air coefficient for all three runs.

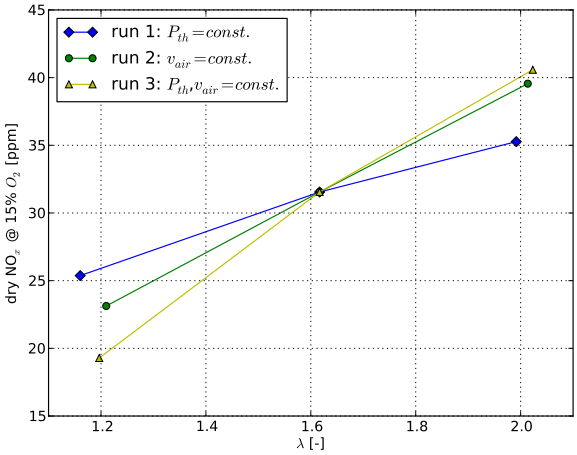

FIGURE 3. NO_x emissions for varying excess air coefficients

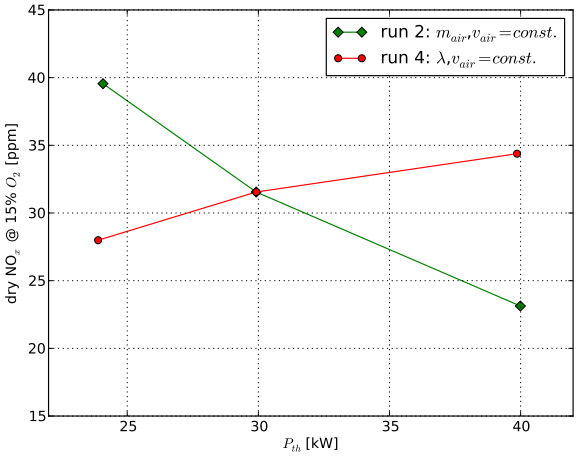

FIGURE 4. NO_x emissions for varying thermal inputs

Fig. 4 shows the NO_x graph for run 2 and 4. For both of them the thermal input was varied between 24.15 and 40.2 kW, while keeping the velocity of the combustion air at a constant value of 115 m/s. For run 2, the combustion air mass flow was kept constant and the excess air coefficient was decreased, respectively. In contrast, for run 4 the excess

air coefficient was kept at a constant value of 1.6, while the combustion air mass flow was varied. Fig. 4 shows that for run 4 the NO_x emissions slightly increase with increasing thermal input. While the difference between the first value of 28 ppm and the final value of 34 ppm is not too big, the graph for run 2 on the other hand, shows a distinctive decrease of NO_x with increasing thermal input and with decreasing excess air coefficient, respectively. This suggests that there is a much stronger influence of the amount of excess air than that of the thermal input.

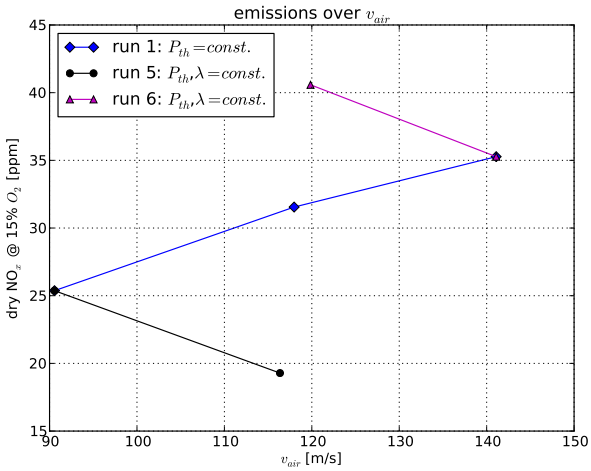

FIGURE 5. NO_x emissions for varying air inlet velocities

Fig. 5 shows the graphs of run 1, 5 and 6. For all of them the inlet velocity of the combustion air was varied, while the thermal input remained constant. Additionally, for runs 5 and 6, the excess air coefficient was kept constant at a value of 1.2 and 2.0, respectively. Fig. 5 shows an increase of NO_x emissions with higher combustion air velocities while the thermal input remains constant for run 1. But then again, for run 1, the excess air coefficient also increases at the same time. For the same amount of excess air (run 5 and 6), even a decrease of NO_x emissions with increasing combustion air velocities can be observed, although this decrease is only 6 ppm each. If run 5 ($\lambda = 1.2$) is compared to run 6 ($\lambda = 2.0$), again, NO_x emissions are lower for the lower excess air coefficient.

The results of Fig. 6 are very similar to those of Fig. 4. It shows the NO_x emissions of run 3 and 4 for varying combustion chamber pressures and for constant combustion air inlet velocities. For run 3 additionally, the thermal input was kept constant and the excess air coefficient was varied between 1.2 and 2.0. For run 4 on the other hand, the excess

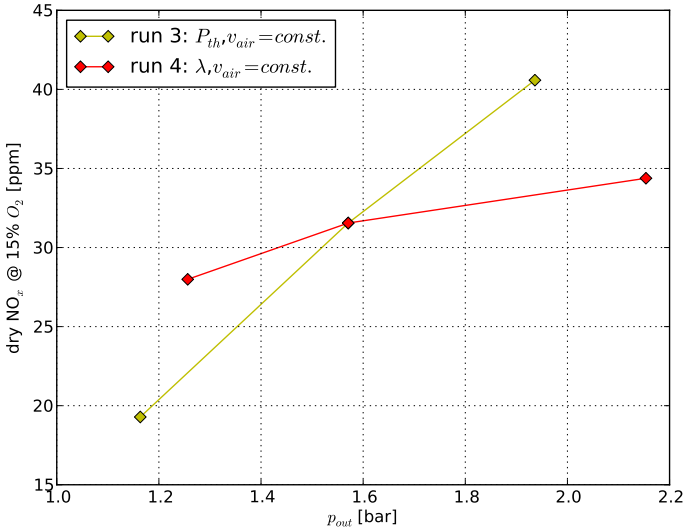

FIGURE 6. NO_x emissions for varying outlet pressures of the combustion chamber

air coefficient was kept at a constant value of 1.6. Although at a first glance, an increase of NO_x emissions with increasing combustion chamber pressure can be observed, this can again be attributed to the fact that the excess air coefficient increases at the same time.

The observed behavior of rising NO_x emissions with increasing excess air coefficients can be explained by the fact that with an increasing amount of excess air inside the combustion chamber, a low oxygen dilution can no longer be achieved. For conventional diffusion flames and low excess air coefficients, high temperature peaks and thus higher NO_x emission values than the ones obtained with this hydrogen combustion chamber can be expected. Nevertheless, values ranging from 19 to 41 ppm are still clearly higher than expected for a combustion chamber operating in pure flameless or MILD combustion mode. This might be attributed to the fact that for all operating conditions, the flame is directly attached to the air inlet, as will be discussed in the next section (Fig. 11). Thus, a sufficient mixing of combustion air and fuel is not possible in this area for this combination of combustion chamber geometry and fuel type. As a consequence of the rich combustion conditions surrounding the air jet in the first part of the combustion chamber, very high temperatures in this area can be expected, leading to an enhanced NO formation via the thermal pathway.

In Fig. 7 the graphs of the liner back wall temperatures, as measured with the probes T2 to T6 (Fig. 1), are shown for run 2. As expected, the temperature profile is highest for the lowest excess air coefficient, which is equivalent to the highest thermal input of run 2. The lowest measured

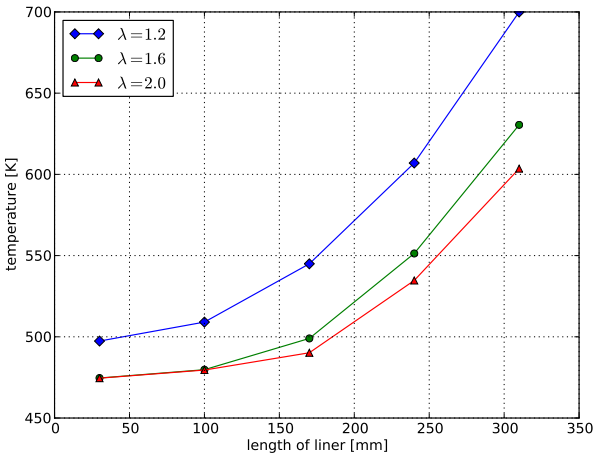

FIGURE 7. Temperature profile across the liner back wall for run 2

value is 475 K ($\lambda = 1.6$ and 2.0) and the highest value is 700 K ($\lambda = 1.2$).

In Tab. 2, the calculated adiabatic temperature (T_{ad}) and the measured exhaust temperature (T_{exh}, measured with probe T7) are shown for run 2. ΔT_1 refers to the temperature difference of T_{ad} and T_{exh}, while ΔT_2 refers to the temperature difference of T_{exh} and T_{air} and is relevant for determining the combustion regime. The temperature difference ΔT_1 for test run 2 is 735 K for $\lambda = 2.0$, and for $\lambda = 1.2$ even 1034 K below the expected adiabatic temperature. Thus, the measures taken to obtain reduced temperature peaks and a reduced overall temperature by air cooling the liner and recirculating the exhaust gases are showing the desired effect. The values of ΔT_1 also correlate with the heat loss of the combustion. But since in this setup the heat is transferred to the cooling air surrounding the combustion chamber, the energy is not entirely lost to the system.

TABLE 2. Run 2: Difference between the calculated adiabatic temperature and the measured exhaust temperature

λ	$T_{air}[K]$	$T_{ad}[K]$	$T_{exh}[K]$	$\Delta T_1[K]$	$\Delta T_2[K]$	$T_{ai} = 865\ K$
1.2	400	2322	1288	1034	888	$\Delta T_2 > T_{ai}$
1.6	400	1961	1110	851	710	$\Delta T_2 < T_{ai}$
2.0	400	1716	981	735	581	$\Delta T_2 < T_{ai}$

According to Cavaliere and de Joannon [12], a combustion regime can be referred to as 'MILD', when the reactant mixture's inlet temperature is above its autoignition temperature and the maximum temperature increase is lower than the mixture's autoignition temperature in Kelvin. To allow the identification of the combustion regime according to this postulation, the autoignition temperatures inside the hydrogen combustion chamber for the present operating conditions were computed with a zero–dimensional perfectly stirred adiabatic constant pressure reactor using Cantera [22]. The residence time was assumed to be constant with 1.13 s, because the air velocity is constant for run 2. The autoignition temperature was detected by increasing the initial temperature of the reactor to the point at which the temperature inside the reactor became significantly larger than the initial temperature after 1.13 s had elapsed. This resulted in autoignition temperatures ranging from 860.2 K to 867.6 K for run 2, depending on the excess air ratio. Because the autoignition temperature depends clearly on the residence time and the differences between the autoignition temperatures of run 2 are not huge, an approximate mean value of 865 K was chosen. This suggests that for excess air coefficients 1.6 and 2.0, the combustion chamber was operating under MILD combustion conditions, whilst for an excess air coefficient of 1.2, the temperature increase in the combustion chamber is only 23 K above Cavaliere's and de Joannon's definition of MILD combustion. Furthermore, one should also keep in mind that in run 2, the lowest excess air ratio comes along with the highest thermal input of 40.2 kW.

NUMERICAL RESULTS

Fig. 8 shows the numerically computed magnitude of the velocity inside the combustion chamber. On the lower

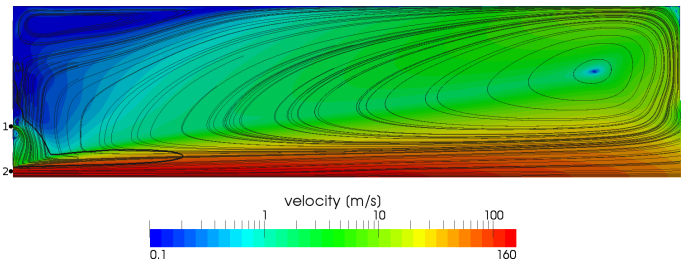

FIGURE 8. Velocity magnitude. The black lines represent the stream lines, whereas the bold black line indicates the stoichiometric mixture. 1...hydrogen inlet; 2...air inlet

part of the left side where the fuel and the air inlets are lo-

cated, the stream lines show that the hydrogen jet is drawn to the air jet immediately after entering the combustion chamber. This can be attributed to the fact that the velocity of the hydrogen jet is distinctly lower than that of the air jet. Fig. 8 also shows the large exhaust gas recirculation zone formed in the upper half, which is a prerequisite for achieving low NO_x emissions with this hydrogen combustion chamber.

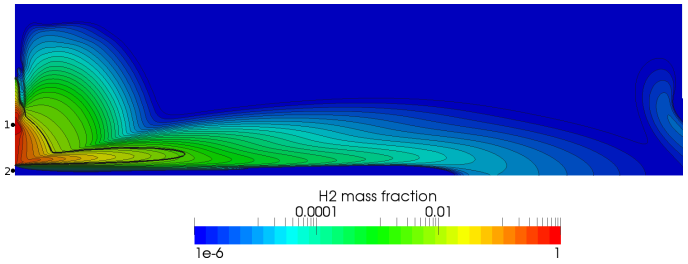

FIGURE 9. Hydrogen mass fraction distribution. The thin black lines represent the isolines of the H_2 mass fraction, whereas the bold black line indicates the stoichiometric mixture. 1...hydrogen inlet; 2...air inlet

In Fig. 9, the distribution of the hydrogen mass fraction inside the combustion chamber is shown using a logarithmic scale. Once again, one can see that the main part of the hydrogen jet is immediately drawn to the air jet below. But additionally, in the middle of the left side, a rather large area is located where hydrogen is present. This can be attributed to the high diffusivity of hydrogen and the low velocity magnitude (below 1 m/s) in this area rather than to convective effects. Thus, a rather big area can be detected, which is located close to the left side wall of the combustion chamber, where a lean combustible mixture is present. Additionally, the CFD result suggests that at the combustion chamber exit, hydrogen is present below 10 ppm. This indicates a combustion efficiency of nearly 100%.

The mass fraction of OH radicals inside the combustion chamber (as shown in Fig. 10 with a logarithmic scale) can be directly linked to the shape of the reaction zone and also indicates its location, allowing conclusions concerning the MILD combustion regime. In the whole area of positive axial velocity, indicated by the streamlines in Fig. 10, between the injectors and the combustion chamber exit, an elevated mass fraction of OH radicals can be found. This indicates that the combustion takes place in this conical area. Only directly at the left wall, between the hydrogen and the air inlet, where the conditions are too rich, and in the core of the air jet, where the conditions are too lean, no OH radicals can be found. The highest mass fraction of OH radicals can

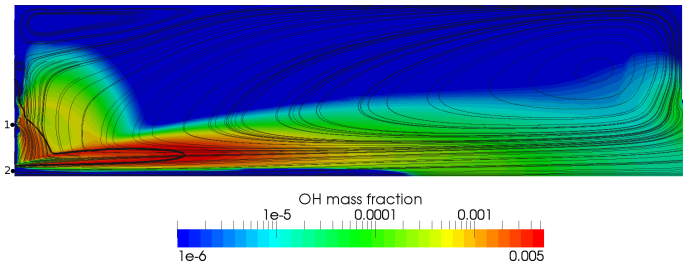

FIGURE 10. OH radical mass fraction distribution. The thin black lines represent the streamlines, whereas the bold black line indicates the stoichiometric mixture. 1...hydrogen inlet; 2...air inlet

be seen in the area above the main air jet, around the bold line indicating stoichiometric combustion conditions. Additionally, as already suggested by Fig. 9, also in the area of hydrogen diffusion at the upper left side of the combustion chamber, a broad and reasonably evenly distributed reaction zone can be observed, as is typically expected of the MILD combustion regime. The area of the OH radicals in this region is not as stretched as the area of the hydrogen. Thus, when the recirculated fluid moves towards this zone, at first there are no OH radicals present. Only after moving further into this zone, the occurrence of OH radicals can also be observed. This suggests, that autoignition is taking place at the rim of the area of hydrogen diffusion.

FIGURE 11. Picture of the hydrogen flame made with a CCD camera. Air and fuel inlets can be seen on the left side of the picture. The viewing direction is not perpendicular to the window.

Fig. 10 also correlates very well with the visible flames observed during the experiments through the viewing window. One picture taken during run 0 is shown in Fig. 11. Obviously, not an entirely flameless combustion mode was

achieved, unlike for the original methane combustion chamber [16,17]. One can clearly see that the flame already starts directly at the burner, with a blue flame jet being formed in the center. Directly at the burner, small bluish flames burn from the hydrogen inlet towards the air jet. This correlates with the rich conditions in Fig. 9 and Fig. 10, which show a very rich, but already combustible mixture for this region and a distinctive reaction zone with an elevated mass fraction of OH radicals, respectively. The predominant blue color seen in Fig. 11 is not unusual for hydrogen flames and due to the presence of OH radicals. The small portion of orange flames can be attributed to the presence of unburnt hydrocarbons. These can be explained by the carbon dioxide content of the air. A very small amount of unburnt hydrocarbons might be attributed to the fact that the compressed air is delivered by an oil cooled screw compressor. Even with the equipped filters it is possible that this very small concentration is sufficient for the orange glow. The reason why there is no lifted flame like for the methane combustion is that hydrogen has a comparatively much higher reactivity and a higher flame velocity, respectively. But still, Ayoub et al. [2] have shown that a lifted flame in a 'mild flameless combustion', as they call it, is also possible for hydrogen. One main difference in their experimental setup compared to the investigated one is a much higher fuel to air jet momentum ratio due to the geometrical conditions of their burner. Interestingly, the hydrogen diffusion zone on the upper left side of the combustion chamber, as shown by the CFD calculations, cannot be seen in Fig. 11. This can be interpreted as evidence for the existence of a MILD or flameless combustion regime in this region.

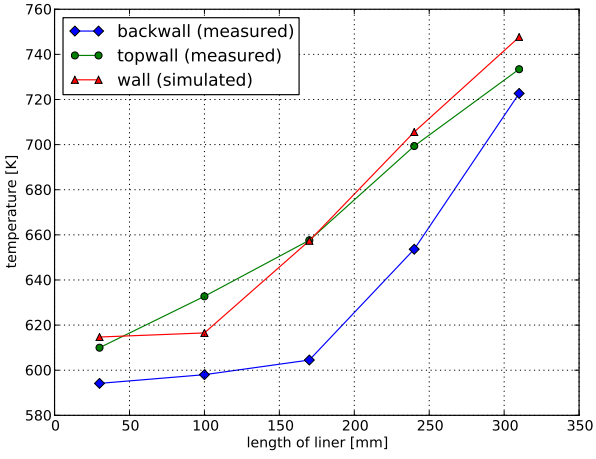

FIGURE 12. Wall temperature profile over the length of the combustion chamber for run 0

In Fig. 12, the results of the experiment (run 0) and the CFD calculation are compared for the wall temperature profile of the combustion chamber. The values of the CFD results (red triangles) are in good agreement with the values measured at the top wall of the combustion chamber (130 x 330 mm; green dots), with the biggest deviation being less than 20 K at a liner length of 100 mm. When compared to the temperatures measured at the back wall of the combustion chamber (240 x 330 mm; blue diamonds), the deviations are bigger, but with a maximum difference of 55 K for the third measuring point, they are still in good accordance. Additionally, the slopes of the CFD results show a very similar behavior to those of the experimental results. Despite the simplified 2D axisymmetric CFD model, these values show that the obtained CFD results are still in good agreement with the conditions of the actual combustion chamber.

CONCLUSION

Different test runs conducted with a hydrogen combustion chamber resulted in NO_x emissions ranging from 19 to 41 ppm (corrected values for 15% oxygen and dry conditions). Although these numbers are lower than expected for conventional diffusion flames, they are definitely higher than can be expected for MILD or flameless combustion. This can be attributed to the fact that the flame is directly attached to the combustion chamber inlet. Thus, in this region the combustion air and the fuel are not yet well mixed. As a consequence, lean conditions are prevailing around the air jet which promote a distinctive NO formation via the thermal pathway.

As reported in literature, for a successful low NO_x combustion concept with a large amount of internal exhaust gas recirculation, the ratio between the fuel and the air jet momentum is crucial. As was able to be shown, this ratio strongly depends on the fuel and has a distinctive impact on the occurrence of the flame and oxidation region, respectively. If the fuel to air jet momentum ratio is too low, the distance between combustion chamber inlet and oxidation zone will be reduced accordingly. Thus, the mixing of fuel and combustion air and recirculated exhaust gases will be worse, resulting in higher NO_x emissions. For hydrogen with its high reactivity and large flammability limits, also a higher fuel to air jet momentum ratio is needed than for methane.

The evaluation of the conducted test runs have shown that NO_x emissions seem to be more or less independent of combustion air velocity and thermal input for constant excess air ratios, while they increase with increasing excess air ratios when other important parameters are kept constant. This can be attributed to the fact that for higher excess air

ratios, the oxygen concentration in the recirculated exhaust gases is also increasing. Thus, the low oxygen dilution of fuel and combustion air cannot be obtained as extensively as for a combustion mode with lower excess air ratios.

A hydrogen burning combustion chamber was designed by scaling an existing methane MILD combustion chamber with the help of dimensionless length ratios. The experimental and numerical investigation of this combustion chamber have both shown that the oxidation zone in the case of hydrogen combustion is more or less attached to the front wall. In order to increase the fuel to air jet momentum ratio, the number of hydrogen fuel injections will be reduced to eight, four and two respectively, and the effect on NO_x emissions will be investigated within the next experimental study.

ACKNOWLEDGMENTS

This work was financed by the national project 'Hy4JetEngines' as part of the 'Austrian Aeronautics Programme TAKE OFF' of the Austrian Research Promotion Agency (FFG). Special thanks goes to Kurt Eckerstorfer whose commitment permitted the combustion chamber's assembly in recordbreakingly time.

NOMENCLATURE

ΔT_1	$T_{ad} - T_{exh}$
ΔT_2	$T_{exh} - T_{air}$
λ	excess air coefficient
$\dot{m}_{air}$	mass flow of the combustion air
$\dot{m}_{fuel}$	mass flow of the fuel
p_{out}	pressure after the combustion chamber
P_{th}	thermal input
T_{ad}	adiabatic flame temperature (calculated)
T_{ai}	auto ignition temperature of the mixture
T_{air}	temperature of air at inlet
T_{exh}	exhaust gas temperature at combustion chamber exit
v_{air}	velocity of air at inlet
v_{fuel}	velocity of fuel at inlet

REFERENCES

[1] Joos, F., 2006. *Technische Verbrennung*, 1 ed. Springer-Verlag.

[2] Ayoub, M., Rottier, C., Carpentier, S., Villermaux, C., Boukhalfa, A., and Honoré, D., 2012. "An experimental study of mild flameless combustion of methane/hydrogen mixtures". *International Journal of Hydrogen Energy,* ***37***(8), pp. 6912–6921.

[3] Warnatz, J., Maas, U., and Dibble, R. W., 2006. *Combustion: physical and chemical fundamentals, modeling and simulation, experiments, pollutant formation.* Springer.

[4] Skottene, M., and Rian, K. E., 2007. "A study of NO_x formation in hydrogen flames". *International Journal of Hydrogen Energy,* ***32***(15), pp. 3572–3585.

[5] Wünning, J., and Wünning, J., 1997. "Flameless oxidation to reduce thermal no-formation". *Progress in energy and combustion science,* ***23***(1), pp. 81–94.

[6] Wünning, J. G., 2004. "Flameless combustion and its applications". *Natural Gas Technologies. Orlando (USA),* ***30***.

[7] Wuenning, J. G., 2008. "Flameless oxidation in gas fired radiant tubes". In 7th High Temperature Air Combustion and Gasification International Symposium, Vol. 2, p. 4.

[8] Arghode, V. K., and Gupta, A. K., 2011. "Hydrogen addition effects on methane–air colorless distributed combustion flames". *International Journal of Hydrogen Energy,* ***36***(10), pp. 6292–6302.

[9] Arghode, V. K., Gupta, A. K., and Bryden, K. M., 2012. "High intensity colorless distributed combustion for ultra low emissions and enhanced performance". *Applied Energy,* ***92***, pp. 822–830.

[10] Gupta, A. K., 2000. "Flame characteristics and challenges with high temperature air combustion". In Proccedings of 2000 International Joint Power Generation Conference, Miami Beach, Florida, ASME, pp. 1–18.

[11] De Joannon, M., Langella, G., Beretta, F., Cavaliere, A., and Noviello, C., 2000. "Mild combustion: Process features and technological constrains". *Combustion science and technology,* ***153***(1), pp. 33–50.

[12] Cavaliere, A., and de Joannon, M., 2004. "Mild combustion". *Progress in Energy and Combustion Science,* ***30***(4), pp. 329–366.

[13] Sorrentino, G., de Joannon, M., and Cavaliere, A., 2010. "Effect of hot diluted fuel flow on reactive structures in mild combustion". *Proc Technol Sust Energ. doi,* ***10***.

[14] Eichler, C., Baumgartner, G., and Sattelmayer, T., 2011. "Experimental investigation of turbulent boundary layer flashback limits for premixed hydrogen-air flames confined in ducts". *Proceedings of ASME Turbo Expo 2011, Vancouver, British Columbia, Canada, GT2011-45362.*

[15] Veríssimo, A., Rocha, A., and Costa, M., 2011. "Operational, combustion, and emission characteristics of a small-scale combustor". *Energy & Fuels,* ***25***(6), pp. 2469–2480.

[16] Veríssimo, A., Rocha., A., and Costa, M., 2013. "Importance of the inlet air velocity on the establishment

of flameless combustion in a laboratory combustor". *Experimental Thermal and Fluid Science,* ***44***, pp. 75–81.

[17] Veríssimo, A., Rocha, A., and Costa, M., 2012. "Experimental study on the influence of the thermal input on the reaction zone under flameless oxidation conditions". *Fuel Processing Technology.*

[18] Borm, O., 2014. "Evaluation of gaseous emissions from hydrogen combustion aircraft engines". *Proceedings of ASME Turbo Expo 2014, Düsseldorf, Germany, GT2014-25470.*

[19] Fukumoto, K., and Ogami, Y., 2012. "Simulation of H_2-air non-premixed flame using combustion simulation technique to reduce chemical mechanisms". *Fluid Dynamics, Computational Modeling and Application, Dr. L. Hector Juarez (Ed.), ISBN: 978-953-51-0052-2, 357-380.*

[20] Mechanism library. `http://www2.galcit.caltech.edu/EDL/mechanisms/library/library.html` - last checked: 2013-12-17.

[21] Allen, M. T., Yetter, R. A., and Dryer, F. L., 1995. "The decomposition of nitrous oxide at $1.5 \leq P \leq 10.5\,atm$ and $1103 \leq T \leq 1173\,K$". *International journal of chemical kinetics,* ***27***(9), pp. 883–909.

[22] Cantera, 2.0. `https://code.google.com/p/cantera/` - last checked: 2013-10-23.